Acta Pharmaceutica Sinica B 2022;12(5):2494–2505

Chinese Pharmaceutical Association
Institute of Materia Medica, Chinese Academy of Medical Sciences

Acta Pharmaceutica Sinica B

www.elsevier.com/locate/apsb
www.sciencedirect.com

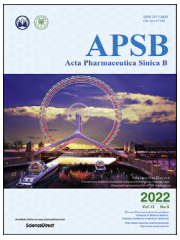

ORIGINAL ARTICLE

Tetrahedral DNA nanostructures synergize with MnO_2 to enhance antitumor immunity *via* promoting STING activation and M1 polarization

Siping Liang[a,†], Jiaying Li[b,†], Zhengyu Zou[a], Miao Mao[c], Siqi Ming[a], Fan Lin[c], Ziyan Zhang[c], Can Cao[a], Jinyu Zhou[a], Yuanqing Zhang[c,*], Jiaping Li[d,*], Minhao Wu[a,*]

[a]*Zhongshan School of Medicine, Sun Yat-sen University, Guangzhou 510080, China*
[b]*Department of Laboratory Medicine, Guangdong Second Provincial General Hospital, Guangzhou 510317, China*
[c]*Guangdong Key Laboratory of Chiral Molecule and Drug Discovery, School of Pharmaceutical Sciences, Sun Yat-sen University, Guangzhou 510006, China*
[d]*Department of Interventional Oncology, The First Affiliated Hospital, Sun Yat-sen University, Guangzhou 510080, China*

Received 23 August 2021; received in revised form 8 October 2021; accepted 18 November 2021

KEYWORDS

Tetrahedral DNA nanostructure;
Manganese;
MnO_2;
STING;
M1 polarization;
Antigen presentation;
Anti-tumor immunity;
Cancer therapy

Abstract Stimulator of interferon genes (STING) is a cytosolic DNA sensor which is regarded as a potential target for antitumor immunotherapy. However, clinical trials of STING agonists display limited anti-tumor effects and dose-dependent side-effects like inflammatory damage and cell toxicity. Here, we showed that tetrahedral DNA nanostructures (TDNs) actively enter macrophages to promote STING activation and M1 polarization in a size-dependent manner, and synergized with Mn^{2+} to enhance the expressions of IFN-β and iNOS, as well as the co-stimulatory molecules for antigen presentation. Moreover, to reduce the cytotoxicity of Mn^{2+}, we constructed a TDN–MnO_2 complex and found that it displayed a much higher efficacy than TDN plus Mn^{2+} to initiate macrophage activation and anti-tumor response both *in vitro* and *in vivo*. Together, our studies explored a novel immune activation effect of TDN in cancer therapy and its synergistic therapeutic outcomes with MnO_2. These findings provide new therapeutic opportunities for cancer therapy.

*Corresponding authors. Tel./fax: +86 20 87334049 (Minhao Wu).
E-mail addresses: zhangyq65@mail.sysu.edu.cn (Yuanqing Zhang), lijiap@mail.sysu.edu.cn (Jiaping Li), wuminhao@mail.sysu.edu.cn (Minhao Wu).
[†]These authors made equal contributions to this work.
Peer review under responsibility of Chinese Pharmaceutical Association and Institute of Materia Medica, Chinese Academy of Medical Sciences.

https://doi.org/10.1016/j.apsb.2021.12.010

1. Introduction

The host anti-tumor immunity is mainly dependent on the T cell-mediated adaptive immunity. However, innate immunity mediated by antigen-presenting cells (APCs) like macrophages and dendritic cells (DCs) as well as innate lymphocytes like natural killer (NK) cells, also plays a critical role in initiating the host defense against tumor cells[1−3]. Currently, PD-1/PD-L1 immune checkpoint blockade (ICB) therapy enhances the tumor-specific adaptive immunity mediated by tumor-infiltrating lymphocytes, and has been demonstrated as a powerful strategy for clinical treatment of various cancer types[4,5]. However, only 20%−40% of cancer patients respond to the treatments and even fewer patients achieve durable remission, due to inadequate innate immune activation[6]. In this regard, new strategies to effectively kill tumor cells are needed for tumor therapy.

The immunosuppressive tumor microenvironment (TME) is caused by a high density of immunosuppressive cells, including tumor-associated macrophages (TAMs), myeloid-derived suppressor cells (MDSCs), regulatory T cells (Tregs) and exhausted cytotoxin lymphocytes (CTLs)[7]. TAMs largely express an alternatively activated (or M2) phenotype, which promote tumor progression. Therefore, it is of great significance to reprogram TAMs towards a tumor-killing M1 type. The strategy can facilitate the solution of low immune response of adaptive immunity. Clinical investigations also show that the accumulation of proinflammatory M1 TAMs is associated with longer survival in patients suffering from some solid tumors[8].

Recent studies have confirmed the essential role of type I interferons for immune responses to eradicate tumor cells. Interferons trigger transcription of diverse genes, which results in both direct (on tumor cells) and indirect (through immune regulations of macrophages, DCs, T cells, NK cells) tumor-killing effects[9]. Stimulator of interferon genes (STING) is a cytosolic DNA sensor that is highly expressed in APCs, and functions to recognize certain types of DNA, such as the uptake of tumor-derived DNA by APCs. Activation of STING subsequently induced the production of IFN-β and interferon-stimulating genes (Isgs), as well as NF-κB-dependent pro-inflammatory cytokines[10]. It is well known that STING/type I IFN pathway is critical in anti-viral response and autoimmunity[11]. Recently, it is also reported that activation of STING/IFN-β promotes the host anti-tumor immunity[12]. Preclinical studies have demonstrated that treatment with the STING agonist cGAMP suppresses tumor growth by promoting antigen presentation and recruiting $CD8^+$ T cells to the TME[13]. Interestingly, recent advances reveal that manganese (Mn^{2+}) dramatically enhances the host anti-tumor immune responses mediated by STING/type I IFN pathway[14]. However, the dosage of manganese ions application *in vivo* needs attention due to its neurotoxicity[15]. To date, the results of clinical trials for STING agonists in cancer therapy are still unsatisfactory, due to the poor penetration efficiency of current STING agonists as well as the inflammatory side-effects prone to occur[16]. In this regard, scientists put many efforts to develope anti-tumor therapy based on optimal STING activation strategies, with higher efficiency and fewer side-effects.

DNA nanostructures were first introduced by Seeman[17] in 1980s. Since then, numerous DNA nanostructures are constructed and applied in drug delivery or bioengineering. Among these nanostructures, tetrahedral DNA nanostructures (TDNs) have showed excellent potential in drug delivery and biomedical treatment. TDNs can easily enter cells without transfection agents or electronic transfection. In addition, TDNs display little cytotoxicity to various cell types[18], and function to influence many cell biological events, such as promoting cell proliferation and migration[19,20], maintaining the chondrocyte phenotype[21], regulating anti-oxidative activity[22]. However, the function of TDNs on host immune response remains largely unknown.

In this study, we demonstrated that TDNs promoted the activation of STING/type I IFN pathway in macrophages, and induced M1 polarization. Then we explored the size effect of TDNs and found that T17 (TDN with 17 bp side length) activated macrophages with the best efficiency. Moreover, *in vitro* and *in vivo* studies showed a synergy of T17 and manganese in augmenting IFN-β production and M1 polarization as well as anti-tumor immune responses. Importantly, T17-MnO_2 (release Mn^{2+} intracellularly) displayed much stronger effects than T17 plus Mn^{2+} in macrophage activation and anti-tumor immunity. These findings identify a novel biological function of TDNs, which may provide potential strategies for cancer immunotherapy.

2. Materials and methods

2.1. Reagents

All DNA single-strands of TDNs used in this work were synthesized by Sangon Biotech (Shanghai, China); TE and TM buffer were purchased from Sangon Biotech (Shanghai, China); Cell Counting Kit-8 was purchased from Glpbio (GK10001, Montclair, CA, USA); TRIzol was purchased from Invitrogen (15596018, Carlsbad, CA, USA); Reverse Transcriptase, GoTaq qPCR Master Mix and Lactate Dehydrogenase Assay Kit were purchased from Promega (M1705, A6002, G1780, Madison, WI, USA).

2.2. Studies in animals

Female C57BL/6J(B6) mice (age, 6−8weeks; body weight, ~20 g) were purchased from the Animal Supply Center of Sun Yat-sen University. *Tmem173*$^{-/-}$ (STING knockout) mice were purchased from Model Animal Research Center of Nanjing University. All experiment protocols were approved by the Ethics Committee Board for Human and Animal Experiments in Zhongshan School of Medicine of Sun Yat-sen University. The procedure was performed in accordance to the National Commission for the Protection of Subjects of Biomedical and Behavioral Research guidelines for animal experiments. All efforts were made to minimize suffering.

2.3. Murine tumor models

Hepa1-6 cells were cultured in Dulbecco's modified Eagle's medium (DMEM) supplemented with 10% FBS and 100 IU/mL

penicillin/streptomycin. Hepa1-6 cells (2.5×10^5) resuspended in 100 μL of 0.9% NaCl were injected subcutaneously into C57BL/6J(B6) mice. To examine the antitumor function of different treatment strategies, tumors were treated *via* intratumoral injection with 100 μL of either vehicle control (0.9% NaCl), Mn^{2+} (50 mmol/L), MnO_2 (2 mmol/L), T17 (3 μmol/L), T17 plus Mn^{2+} or T17-MnO_2 (first treatment on Day 8, second treatment on Day 14, third treatment on Day 17). Tumor growth was monitored every other day after treatment. Tumor volume was calculated by the following Eq. (1):

$$\text{Tumor volume} = 0.5 \times \text{Length} \times \text{Width}^2 \quad (1)$$

Tumor sections were harvested after 12 days' treatment and stained with hematoxylin–eosin staining (H&E).

2.4. Tumor-infiltrating leukocytes analysis

Tumors were isolated and harvested on Day 12 after indicated treatments, and then processed with a tissue processor (Miltenyi, Gentle MACS Octo, Bergisch Gladbach, Germany), and digested in a solution of 1 mg/mL Collagenase Type II (Gibco, 17101015, Carlsbad, CA, USA) in RPMI-1640 media (Gibco, A1049101) with a constant temperature shaker at 37 °C for 1 h. Then cells were filtered through a 70 μm filter. Single-cell suspensions were stained with indicated antibodies and then accessed by flow cytometry. The data was analyzed by FlowJo v10.0 (Becton, Dickinson and Company, Ashland, OR, USA).

2.5. Preparation of TDNs

Specific DNA single strands of TDNs as shown in Table S1 were mixed in the same concentration in TM buffer (10 mmol/L Tris−HCl, pH 8.0, 50 mmol/L $MgCl_2$). The mixture was heated to 95 °C for 10 min and then rapidly cooled to 4 °C for 10 min. Agarose gel electrophoresis was used to demonstrate the successful synthesis of TDNs.

2.6. Assembly and characterization of T17-MnO_2

A mixed aqueous solution of 20 mL of tetramethylammonium hydroxide (0.6 mol/L) and H_2O_2 (3 wt%) was added to 10 mL of $MnCl_2$ (0.3 mol/L) solution. The mixture was stirred at room temperature overnight to obtain MnO_2. The prepared MnO_2 was centrifuged at 2000 rpm (Eppendorf, 5424, Hamburg, Germany) for 20 min and washed with a large amount of distilled water and methanol, and then dried at 60 °C. Then 10 mg of the sample was dispersed in 10 mL of water, and the MnO_2 nanosheets were obtained by ultrasonic treatment for 4 h. T17 was incubated with MnO_2 nanosheets at room temperature for 2 h to obtain T17-MnO_2. The synthesis of T17-MnO_2 was characterized by the nanoparticle size analyzer.

2.7. Cell isolation and culture

C57BL/6(B6) mice were sacrificed by cervical dislocation, and the femur and tibia were separated to expose the bone marrow cavity. Washed out the cells from the bone marrow cavity, and lysed the erythrocytes. Then collected the rest bone marrow cells by centrifugation. The collected cells were cultured in 10% FBS DMEM medium containing 30% L929 cell supernatant for 7 days to induce them differentiating into the bone marrow-derived macrophages (BMDMs).

2.8. Activation of T cells in vitro

C57BL/6(B6) mice were sacrificed, and the spleens were isolated and ground. The erythrocytes were lysed, and the rest cells were collected by centrifugation. Biotinylated CD3/CD4/CD8 antibody mixture was added into cells (per 1×10^6 cells in 5 μL) and incubated at room temperature for 15 min. After that, magnetic beads were added into cells (per 1×10^6 cells in 5 μL) and incubated at room temperature for 30 min. The cells were transferred into the flow tube and placed on the magnetic rack, incubated at room temperature for 8 min. The supernatant was carefully absorbed and removed from the magnetic rack. One time sorting buffer was added and gently blown for 10−15 times to resuspend the cells, then put back into the magnetic rack and incubated for 6 min and the $CD3^+/CD4^+/CD8^+$ T cells were obtained. Then T cells and BMDMs were added into 96-well U-bottom plate in a ratio of 2:1 and co-cultured for 3 days.

2.9. Real-time polymerase chain reaction analysis

Total RNA was isolated from cell lysates with TRIzol. Revert aid first strand cDNA synthesis kit was used to prepare cDNA. Then, real-time PCR reactions were performed by CFX96 Real-Time PCR System (Bio-Rad, Hercules, CA, USA). Sequences of primer pairs are listed in Table S2.

2.10. Western blot

Cells were lysed in 1× RIPA lysis buffer with protease and phosphatase inhibitors. And then the proteins were separated by sodium dodecyl sulfate−polyacrylamide gel electrophoresis (SDS-PAGE) and were transferred to polyvinylidene difluoride membranes. The target membranes were incubated with primary antibodies: anti-β-actin (Sigma−Aldrich, A1978, St. Louis, MO, USA), GAPDH (Sigma−Aldrich, G9295), iNOS (CST, 13120, Danvers, MA, USA), Arginase-1 (CST, 93668), phospho-TBK1 (Ser172) (CST, 5483), TBK1 (CST, 38066), phospho-IRF3 (Ser386) (CST, 37829), IRF3 (CST, 11904) overnight at 4 °C, followed by incubation with secondary antibodies. The membranes were visualized with New-SUPER ECL (KeyGEN, KGP1128, Nanjing, China) according to the manufacturer's instructions.

2.11. Flow cytometry analysis

Single-cell suspensions were prepared from BMDMs or fresh mouse tumor tissues. The cell suspension was filtered and stained in PBS containing 1% BSA for 30 min on ice in the dark and then washed and fixed in a solution of 1% paraformaldehyde. The antibodies against following molecules were purchased from BioLegend (Beijing, China): anti-CD11b (101206), F4/80 (123116), CD11c (117318), Ly-6G/Ly-6C (108428), CD3 (100218), CD4 (100406), CD8 (100714), NK1.1 (108728), iNOS (696806), CD69 (104508), CD86 (105014), CD206 (141707), MHCII (107608), PD-1 (135216).

For intracellular cytokine analysis, 3×10^5 cells were seeded in a 96-well plate in DMEM containing 10% FBS and supplemented with PMA/Ionomycin/Brefeldin A cocktail. After 4 h, cells were washed, stained with surface antibodies for 30 min, and

then fixed with fixation buffer and subsequently stained intracellularly with antibodies against IL-1β (Invitrogen, 2016884), IFN-γ (BioLegend, 505808), TNF-α (BioLegend, 506306) and granzyme B (BioLegend, 515408). After 45 min, cells were washed and fixed in a solution of 1% paraformaldehyde.

2.12. *Statistical analysis*

The statistical analysis was conducted by GraphPad Prism/Excel software, and the data were shown as mean ± standard deviation. The difference between the two groups was analyzed by Student's *t*-test, and the difference between multiple groups was analyzed by one-way ANOVA. $P < 0.05$ indicated a statistically significant difference.

3. Results

3.1. *Synthesis and features of TDNs*

As the scheme showed (Fig. 1A), TDNs were synthesized by four single-strand (ss) DNAs that are self-assembled by complementary pairing. The stabilities of assembled TDNs *vs* dsDNA in the presence of serum were examined, and the results showed that structured TDNs displayed more stabilities than dsDNA (Fig. 1C).

It has been reported that TDNs can enter the cell without transfection agents or electronic transfection, by virtue of their unique three-dimensional structure. To access whether the TDNs enter the cell in a size-dependent manner, we next assembled five TDNs in different sizes, namely T7, T13, T17, T26, and T37, respectively, based on the length of ss DNAs assembling the TDNs. Agarose gel electrophoresis data demonstrated the successful assembly of the indicated TDNs with different sizes (Fig. 1B, Fig. S1A–E). Then we synthesized TDNs with one Cy5-labelled ss DNA and three unlabeled ss DNAs using the same nuclear acid sequence as shown in Table S1, and traced their cellular uptake by BMDMs. At 1 and 3 h after incubating with Cy5-TDNs in different sizes, including T7, T13, T17, T26 and T37, the fluorescence of intracellular Cy5-TDNs in BMDMs were examined by flow cytometry. The cellular uptake efficiency of the indicated TDNs in different sizes was comparable, and more than 95% BMDMs were Cy5-TDN positive after 3 h incubation (Fig. 1D). To explore whether tetrahedral DNA actively or passively enter the macrophages, we synthesized Cy5-labelled ssDNA (Cy5-a) as well as Cy5-ab and Cy5-abc, which is composed of one Cy5-labelled ss DNA plus one or two unlabeled ss DNAs, respectively, under the same conditions as TDNs synthesis, and then traced their cellular uptake by BMDMs. The fluorescence of intracellular Cy5-a, Cy5-ab or Cy5-abc in BMDMs was examined by flow cytometry, and the data showed that less than 15% BMDMs were Cy5 positive after 3 h incubation of the unassembled DNAs above (Fig. 1E), indicating that it is TDNs rather than ssDNA that can actively enter the macrophages.

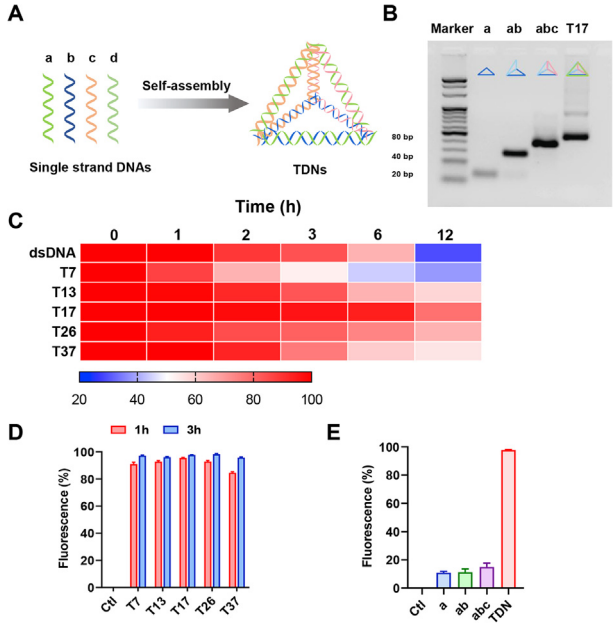

Figure 1 Synthesis and features of TDNs. (A) Schematic diagrams of the assembly of TDNs. (B) The synthesis of TDN with sizes of 17 bp was analyzed by agarose gel electrophoresis, the concentration of agarose gel is 3.5%. (C) Electrophoretic analysis of the stability of TDNs and dsDNAs incubated in serum for 0, 1, 2, 3, 6 and 12 h. The intensity of electrophoretic bands was analyzed by the software ImageJ and displayed in heat map. (D) After treatment of Cy5-labelled TDNs (200 nmol/L) in different sizes with optiMEM for 1 or 3 h, cells were collected and washed for three times, and then detected by flow cytometry. (E) After 3 h incubating with Cy5-a, Cy5-ab or Cy5-abc, cellular uptake of ssDNA and TDNs (200 nmol/L) were detected by flow cytometry. Data are presented as mean ± SD ($n = 3$).

3.2. *T17 activates the STING/IRF3/type I IFN pathway in macrophages and favors M1 polarization*

So far, the biological functions of TDNs are still unclear. Considering TDN is a kind of DNA materials, we next examined whether TDNs can activate the cytosolic DNA sensor and downstream type I IFN pathway, and if so, whether there is a size-dependent effect. Primary mouse BMDMs were incubated with five TDNs with different sizes as mentioned above, and then analyzed for the STING activation and type I IFN production. Among the indicated TDNs, T17 showed the most prominent effects in up-regulating the mRNA expression of *Ifnb* as well as the protein levels of phosphorylated TBK1 and IRF3 (Fig. 2A and B). Therefore, T17 was selected for subsequent experiments. After treatment of T17, cell viability of BMDMs was examined and the results showed that T17 had no cytotoxicity to BMDMs (Fig. 2C). It is reported that TDNs up-regulated the mRNA level of *Inos* and *Tnfa* in mouse macrophage-like RAW264.7 cells[22]. Our PCR data showed that T17 treatment in primary BMDMs increased the expression of M1-related genes, including *Stat1*, *Inos*, *Tnfa*, *Il1b*, *Cd86* and *Cd74*, but decreased the expression of M2-related genes like *Arg1* and *Cd206*. The expression of the genes relating to activate STING/type I IFN pathway was also enhanced in T17-treated *vs* control group (Fig. 2D). Western blot results further confirmed that TDN-enhanced INOS expression in macrophages in a size-dependent manner, and T17 showed the best effects in INOS induction (Fig. 2B). T17 up-regulated the protein level of INOS and down-regulated ARG-1 in BMDMs (Fig. 2E). Flow cytometry data also demonstrated that T17 increased the production of INOS, TNF-α and IL-1β by BMDMs (Fig. 2F, Fig. S2A–C). To further examine whether the T17-promoted M1 polarization depends on STING signaling, WT and STING KO (*Tmem173*$^{-/-}$) BMDMs were treated with T17, and then analyzed for M1 polarization. Real-time PCR data showed that T17 still promoted *Inos* expression in STING KO BMDMs, although the

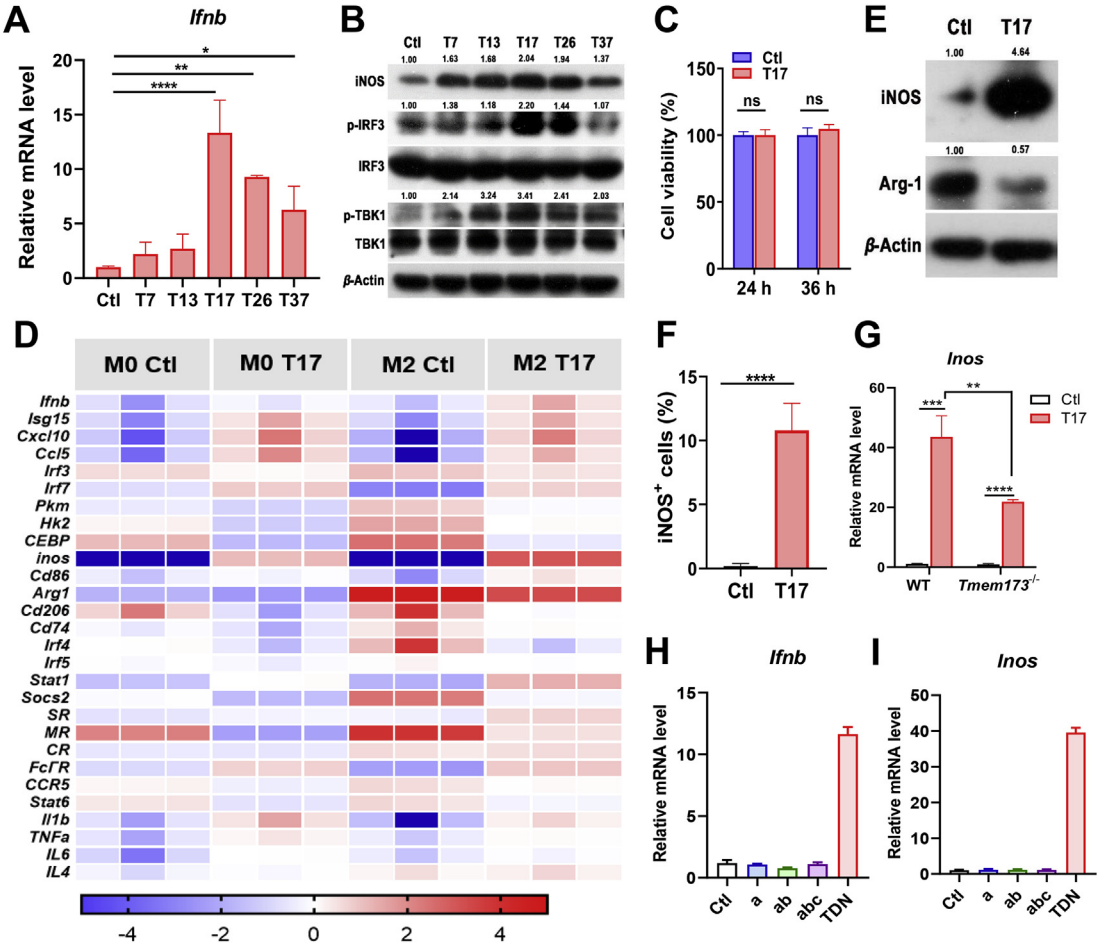

Figure 2 T17 activates the STING/IRF3/IFN-I pathway in macrophages and favors M1 polarization. After treatment of TDNs (200 nmol/L) in different sizes with optiMEM for 3 h, cells were cultured with complete culture medium and collected at 24 h. (A) The mRNA level of *Ifnb* in BMDMs was detected by Real-time PCR (B) and the protein levels of TBK1, IRF3 and INOS in BMDMs were detected by Western blot. After treatment of T17 (200 nmol/L), (C) cell viability of BMDMs was detected by CCK-8 assay, (D) the mRNA levels of the genes in BMDMs were detected by Real-time PCR and displayed by heat map, (E) the protein levels of INOS and ARG-1 in BMDMs were detected by Western blot, (F) and the protein level of INOS was detected by flow cytometry. (G) After treatment of T17 (200 nmol/L), the mRNA level of *Inos* in WT or STING KO (*Tmem173*$^{-/-}$) BMDMs was detected. (H, I) After 3 h incubating with Cy5-a, Cy5-ab or Cy5-abc, the mRNA level of *Ifnb* and *Inos* was detected by Real-time PCR. Data are presented as mean ± SD ($n = 3$). *$P < 0.05$, **$P < 0.01$, ***$P < 0.001$, ****$P < 0.0001$, ns, not significant.

T17-mediated *Inos* increase was much lower than that in WT BMDMs (Fig. 2G), indicating that T17-induced M1 polarization partially depends on STING. Furthermore, we tested the efficiency of synthetic ss DNAs (a, ab, abc) *vs* TDNs in macrophage activation and found that only TDNs can induce the production of *Ifnb* and *Inos*, whereas other ss DNAs failed to activate macrophages (Fig. 2H and I). Since the synthetic TDNs contain little ssDNA, and displayed a high stability during 12 h in the serum (Fig. 1B and C), we speculate that it is TDNs that actively enter the macrophages and induce the macrophages activation. Collectively, these results suggested that T17 promotes the activation of STING/type I IFN pathway and M1 polarization.

3.3. *T17 and manganese ion synergistically enhance the immune response*

Recent studies have suggested that Mn^{2+} and Mg^{2+} promotes the activation of cGAS-STING/type I IFN pathway[23]. Moreover, it is also reported that Ca^{2+} functions as second messenger in mediating signaling transduction[24]. In this regard, we next tested whether T17 cooperates with distinct divalent metal ions to enhance the immune functions of macrophages. After treatment with these three divalent metal ions (Mn^{2+}, Mg^{2+}, Ca^{2+}), the cell cytotoxicity was examined. The results showed that within the concentration of 50 μmol/L, divalent metal ions had no obvious cytotoxicity to BMDMs, while at a concentration of 100 μmol/L, manganese ions exhibited a cytotoxic effect on BMDMs (Fig. S3A). Accordingly, BMDMs were treated with T17 and distinct metal ion solutions within 50 μmol/L. Real-time PCR data showed that only Mn^{2+} significantly up-regulated the mRNA levels of *Ifnb*, *Isg15* and *Inos* in a concentration-dependent manner (Fig. 3A–C). More importantly, the combination of T17 with Mn^{2+} acted synergistically to enhance the activation of STING/type I IFN pathway and M1 polarization (Fig. 3D). Also, the phosphorylation and dimerization of STING protein were detected by Western blot, and the data further confirmed that co-treatment of T17 and Mn^{2+} synergistically induced STING activation (Fig. 3E).

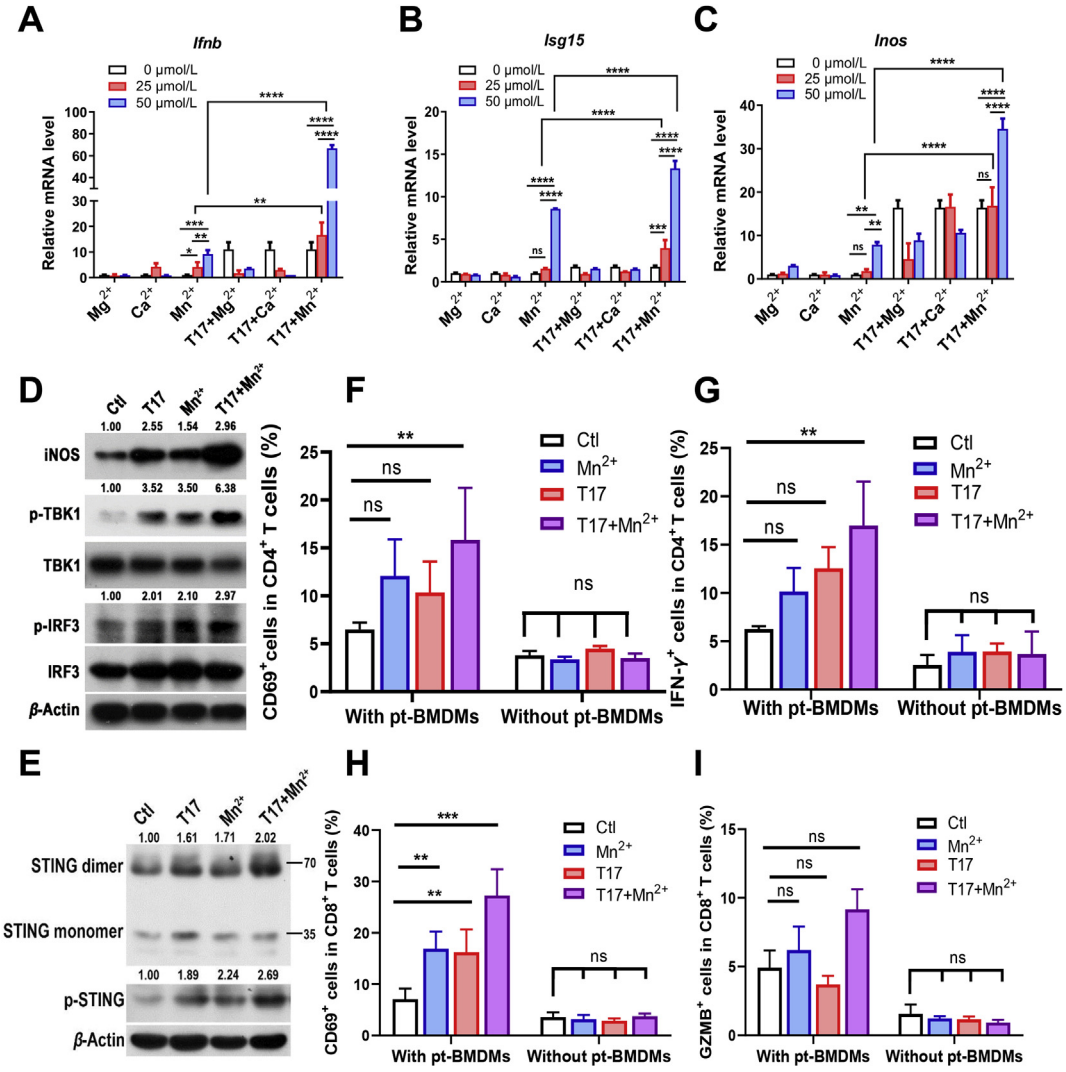

Figure 3 T17 and manganese ion synergistically enhances the immune response. After treatment of different minerals and T17 (200 nmol/L) for 24 h, (A−C) the mRNA levels of *Ifnb*, *Isg15*, *Inos* in BMDMs were detected by Real-time PCR (D, E) and the protein levels of INOS, the phosphorylation of TBK1, IRF3 and STING, the dimerization of STING was detected by Western blot. (F−I) BMDMs were pretreated with T17 (200 nmol/L) and $MnCl_2$ (50 μmol/L) for 24 h (pt-BMDMs), followed by co-culture with T cells for 3 days, or T cells were treated by T17 (200 nmol/L) and $MnCl_2$ (50 μmol/L) directly and then co-cultured with BMDMs for 3 days (without pt-BMDMs), CD69 and IFN-γ in $CD4^+$ T cells, as well as CD69 and granzyme B in CD8+T cells were detected by flow cytometry. Data are presented as mean ± SD ($n = 3$). $^*P < 0.05$, $^{**}P < 0.01$, $^{***}P < 0.001$, $^{****}P < 0.0001$, ns, not significant.

Moreover, the effects of T17 and Mn^{2+} on antigen presentation and T cell activation were investigated. T17 also rapidly entered $CD4^+$ T cells (Fig. S3B) and $CD8^+$ T cells (Fig. S3C). However, direct treatment of T17 and Mn^{2+} in T cells did not promote the expression of CD69 and IFN-γ in $CD4^+$ T cells, or CD69 and granzyme B (GZMB) in $CD8^+$ T cells, suggesting that T17 and Mn^{2+} did not directly influence the T cell function. While after co-culture for 3 days with BMDMs pretreated with Mn^{2+}, T17 or T17 plus Mn^{2+} (pt-BMDMs), the expression levels of the above molecules were slightly increased in T cells when co-cultured with BMDMs pretreated with Mn^{2+} or T17, and dramatically increased in T cells co-cultured with T17 plus Mn^{2+}-pretreated BMDMs (Fig. 3F–I). These results indicated that combination of T17 with Mn^{2+} synergistically improved the antigen presentation activities of BMDMs, thereby leading to the sequential activation of T cells co-cultured with macrophages.

3.4. *T17-MnO_2 enhances the immune response of BMDMs*

Since manganese ions exhibited a cytotoxic effect at a concentration more than 100 μmol/L, we next constructed a MnO_2 nanosheet which can react with intracellular GSH and slowly release Mn^{2+} in the cellular compartment. T17 was adsorbed onto the MnO_2 nanosheet to assemble T17-MnO_2 (Fig. 4A). We characterized the synthesis of T17-MnO_2 by nanoparticle size analyzer. The diameter of T17-MnO_2 was significantly larger than that of T17 and MnO_2 (Fig. 4B). And the electronegativity of T17-MnO_2 was much greater than that of T17 and MnO_2 (Fig. 4C), suggesting that the electronegative DNA structure successfully adsorbed onto the surface of MnO_2 nanosheets. These data indicated the successful synthesis of T17-MnO_2. Next, the cytotoxicity of T17-MnO_2 was examined by detecting the release of LDH from BMDMs after treatment and the results

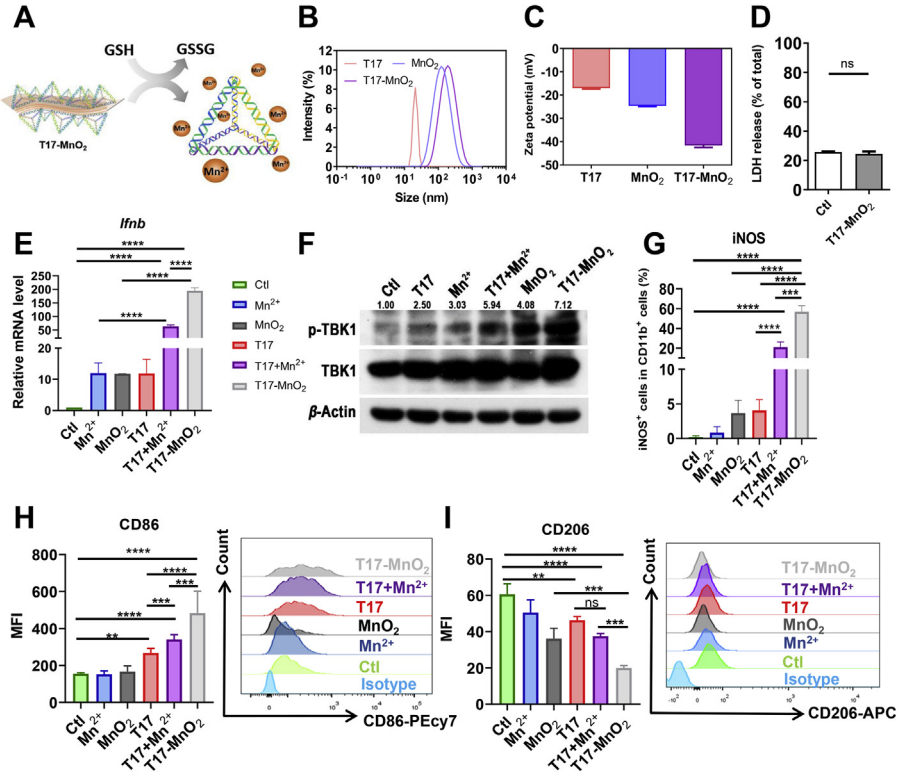

Figure 4 T17-MnO_2 enhanced the immune response of BMDMs. (A) A schematic diagram of the synthesis of T17-MnO_2. (B, C) Particle size distribution and zeta potential of T17-MnO_2 were detected by the nanoparticle size analyzer. (D) LDH release of BMDMs was detected after T17-MnO_2 treatment for 24 h. After treatment of $MnCl_2$ (50 μmol/L), MnO_2 (50 μmol/L), T17 (200 nmol/L), T17+$MnCl_2$, and T17-MnO_2 for 24 h, (E) the mRNA levels of *Ifnb* in BMDMs were detected by Real-time PCR, (F) the protein level of TBK1 in BMDMs was detected by Western blot, (G—I) and the protein levels of INOS, CD86 and CD206 were detected by flow cytometry. Data are presented as mean ± SD ($n = 3$). $^{**}P < 0.01$, $^{***}P < 0.001$, $^{****}P < 0.0001$, ns, not significant.

showed that T17-MnO_2 displayed no cytotoxicity to BMDMs (Fig. 4D). Furthermore, we investigated the potential of T17-MnO_2 on macrophage activation and anti-tumor therapy. Real-time PCR and Western blot data showed that T17-MnO_2 remarkably enhanced the *Ifnb* mRNA expression (Fig. 4E) and TBK1 phosphorylation in BMDMs (Fig. 4F), suggesting that T17-MnO_2 activated the STING/type I IFN pathway in macrophages. In addition, after T17-MnO_2 treatment, the protein level (Fig. 4G and Fig. S4A) and mRNA levels (Fig. S4B) of M1 marker INOS in BMDMs was significantly elevated. Besides, the expression of costimulatory molecules including CD86 (Fig. 4H) and MHCII (Fig. S4C) was increased, while the expression of CD206, a surface marker for M2 macrophages, was significantly reduced (Fig. 4I). These results together confirmed that T17-MnO_2 promoted antigen presentation and favored M1 polarization in macrophages.

3.5. *T17-MnO_2 dramatically improves the anti-tumor response*

Next, we wonder whether T17-MnO_2 play a role in anti-tumor immunity. Considering Hepa1-6 cells have the advantages of short time and high successful rate when used to establish tumor models. Besides, the pathological process of the tumor models is similar to that of its clinical counterpart[25,26]. C57BL/6J (B6) mice were subcutaneously inoculated with Hepa1-6 cells, and then received intratumor injections of vehicle control (0.9% NaCl), Mn^{2+} (50 mmol/L), MnO_2 (2 mmol/L), T17 (3 μmol/L), T17 plus Mn^{2+} or T17-MnO_2 (Fig. 5A). Representative tumor figures and tumor sizes for each group were shown (Fig. 5B and C). Compared with the control group, treatment with Mn^{2+}, MnO_2 slightly reduced the tumor growth, while treatment with T17, T17 plus Mn^{2+} and T17-MnO_2 dramatically suppressed the tumor growth. Meanwhile, the weight change of the mice in each group after the treatment was comparable (Fig. 5D). Moreover, mice-bearing Hepa1-6 xenograft displayed a much stronger efficacy in suppressing tumor growth after treatment with T17-MnO_2, or T17 plus Mn^{2+}, when compared with that in T17-treated group. To be noted, although T17-MnO_2 and T17 plus Mn^{2+} showed potent anti-tumor activities, the usage of Mn^{2+} in T17 plus Mn^{2+} group was twenty-five times more than that in T17-MnO_2 group, indicating that T17-MnO_2 complex had a higher anti-tumor efficacy and less cytotoxicity than free Mn^{2+} plus T17. H&E staining revealed tumor necrosis in the T17-MnO_2 group (Fig. 5E).

Next, we evaluated the role of T17-MnO_2 in host antitumor immune response. Tumor-infiltrating cells from each group were isolated and analyzed by flow cytometry. Intratumoral treatment with T17-MnO_2 slightly increased the percentage of tumor infiltrating neutrophils ($CD11b^+Gr1^+$), but dramatically increased the percentages of antigen-presenting cells including dendritic cells (DCs, $CD11b^+CD11c^+$) and macrophages ($CD11b^+F4/80^+$) (Fig. 6A and Fig. S5A). Additionally, the expression levels of CD86 on the surface of DCs and macrophages were increased after T17-MnO_2 treatment, while the CD206 expression on the surface of macrophages was down-regulated (Fig. S5B–S5D).

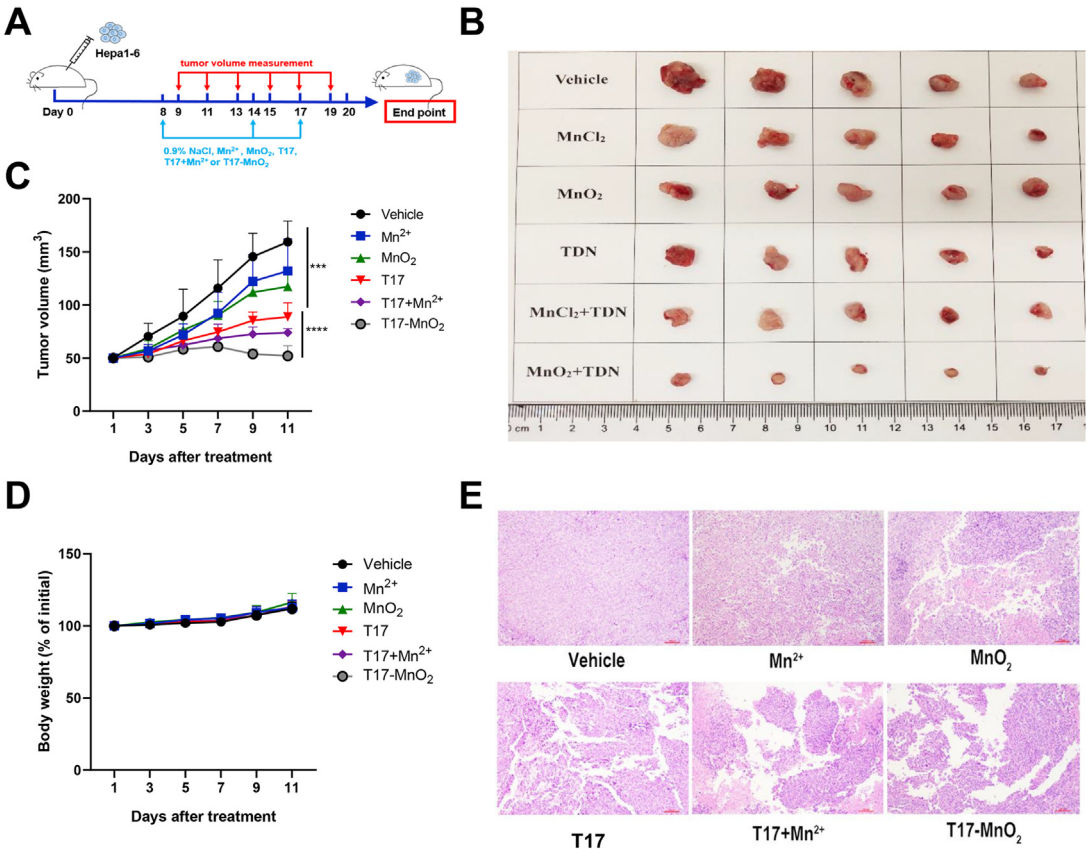

Figure 5 Intratumoral injection of T17-MnO_2 displays potent therapeutic effects. Mice were inoculated with Hepa1-6 cells on Day 0. (A–C) On Days 8, 14 and 17, mice were treated with either vehicle control (0.9% NaCl), Mn^{2+} (50 mmol/L), MnO_2 (2 mmol/L), T17 (3 μmol/L), T17 plus Mn^{2+} or T17-MnO_2 by i.t. administration. (A) A schematic diagram of the tumor model. (B) Photographs of Hepa1-6 tumors on Day 20. (C, D) Tumor size and body weight were recorded every other day after receiving treatment (Days 9, 11, 13, 15, 17 and 19). Tumor growth curve is shown. (E) H&E staining of tumors. Data are presented as mean ± SD ($n = 5$). ****$P < 0.0001$.

T17-MnO_2 also up-regulated the mRNA expression of *Ifnb* and *Inos* in TILs (Fig. S5E and S5F). Moreover, tumor-infiltrating natural killer (NK) cells, $CD4^+$ (helper) and $CD8^+$ (cytotoxic) T cells increased the most in T17-MnO_2-treated mice, among all the indicated groups (Fig. 6B–D and Fig. S6A). And the $CD4^+$ T cells isolated from T17-MnO_2-treated mice contained a higher proportion of effector and memory T cell subsets (Fig. 6E). The proportion of activated lymphocytes among a subpopulation of helper T cells ($CD3^+CD4^+$/$CD3^+CD4^+CD69^+$) and cytotoxic T cells ($CD3^+CD8^+$/$CD3^+CD8^+CD69^+$) was also higher than that of other groups (Fig. S6B and S6C). More importantly, treatment with T17-MnO_2 increased the cytokine production in tumor-infiltrating T cells, including IFN-γ (Fig. 6F) and TNF-α (Fig. S6D) in $CD4^+$ T cells, as well as granzyme B in $CD8^+$ T cells (Fig. 6G), and the expression levels of immune checkpoint programmed death-1 (PD-1) on tumor-infiltrating $CD8^+$ T cells also decreased slightly (Fig. S6E). Taken together, our results demonstrated that T17-MnO_2 induced a potent host anti-tumor immune response and therefore inhibited the tumor growth with a high efficacy.

4. Discussion

Tumor-infiltrating immune cells play a critical role in regulating tumor growth. To date, a variety of anti-tumor immunotherapies have been developed and displayed a great potential in clinical cancer treatment[27]. However, most of the current anti-tumor immune therapies are mainly focused on tumor infiltrating lymphocytes (TILs) and only benefit a small percentage of cancer patients, particularly those with immune active ("hot") tumors. Nonetheless, most of the immune therapies targeting TILs are failed in treating "cold" tumors, in which T cell infiltration is not prevalent and immunosuppressive immune cell infiltration is high[28]. Recent studies have demonstrated the critical role of cGAS-STING/type I IFN pathway in host anti-tumor immunity[10,29,30]. However, clinical trials of the STING agonists, cyclic dinucleotides (CDNs) in tumor therapy do not succeed, due to the poor penetration ability, low stability and inflammatory side effects of CDNs[31]. Thus, the present study was designed to develop a novel anti-tumor immune strategy based on highly efficient activation of STING/type I IFN signaling.

In the present study, we demonstrated that TDNs actively entered the macrophages within a short time period. Moreover, TDNs showed a stronger stability in serum and more resistance to DNase, when compared to classical dsDNAs. So far, a variety of DNA nano structures have been designed and assembled, but only TDNs have been reported to be able to actively enter the cells without transfection, and display little cytotoxicity to various cells[18]. These features endow TDNs a great potential during *in vivo* application. However, most of the studies on TDNs are mainly focused on drug

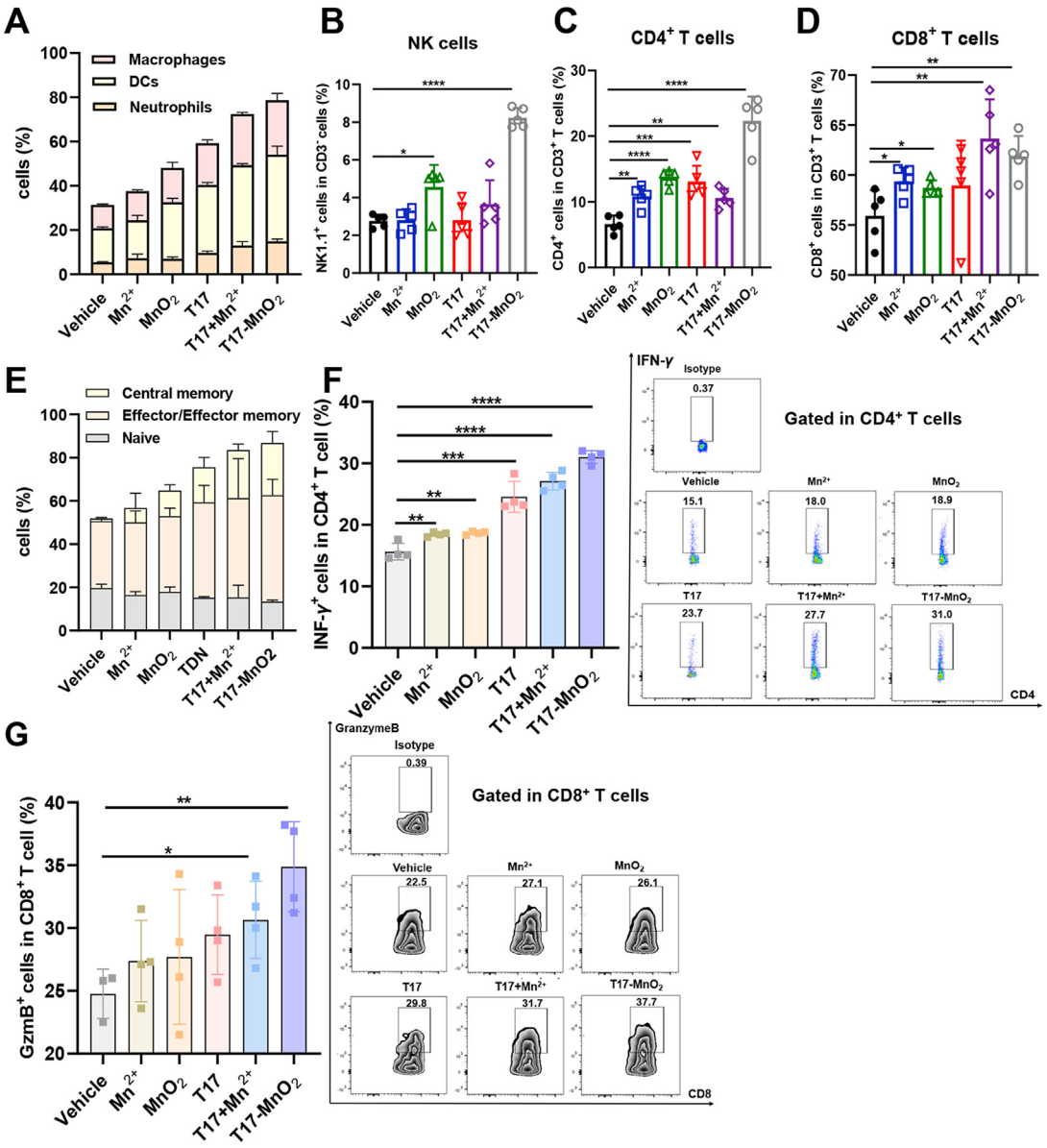

Figure 6 T17-MnO_2 promotes anti-tumor responses by activating both innate and adaptive immunity. Hepa1-6 growth and mice treated with vehicle control (0.9% NaCl), Mn^{2+} (50 mmol/L), MnO_2 (2 mmol/L), T17 (3 μmol/L), T17 plus Mn^{2+} or T17-MnO_2. Mice were sacrificed and tumor-infiltrating leukocytes were analyzed by flow cytometry on Day 20. (A) Percentage of neutrophils ($CD11b^+Gr1^+$), dendritic cells (DCs, $CD11b^+CD11c^+$) and macrophages ($CD11b^+F4/80^+$) were analyzed. (B–D) Tumor-infiltrating $CD4^+$/$CD8^+$ T cells and natural killer (NK) cells. (E) Frequency of naïve cells ($CD44^-CD62L^+$), effector/effector memory cells ($CD44^+CD62^-$) and central memory cells ($CD44^+CD62^+$) in tumor-infiltrating $CD4^+$ T cells. (F) IFN-γ^+ in $CD4^+$ T cells and (G) granzyme B+ in CD8+ T cells. Data are presented as mean ± SD ($n = 4$). $^*P < 0.05$, $^{**}P < 0.01$, $^{***}P < 0.001$, $^{****}P < 0.0001$.

delivery and biosensor detection, whereas the function of TDNs on host immune response remains largely unknown.

Our study demonstrated that TDNs induced STING activation and expression of *Ifnb* and *Isgs*. It is well known that STING directly recognizes CDNs like cGAMP and c-di-GMP with a high affinity[10]. Recently studies demonstrated that cGAMP was transferred to bystander cells *via* VRACs[32]. However, the targetability and drug-loading capacity of cGAMP need to be improved. It has been reported that TDNs can be easily modified with aptamers or peptides to direct specific binding to the targets on tumor sites[33,34]. TDNs also display a potential in drug delivery system, by loading small molecule drugs or chemical inhibitors. In this regard, it is possible to develop TDNs loaded with certain inhibitors (*e.g.*, inhibitors of the NF-κB pathway) to reduce the side effects (*e.g.*, inflammatory cytokine storm) and achieve the best anti-tumor effects. Therefore, using TDNs which can solve these problems is a promising, relative low-cost method to activate STING pathway. Moreover, STING also functions as a central molecule of various cytosolic DNA sensors to induce type I IFN production. In addition to CDNs, STING activation may also be triggered by many other kinds of DNAs, including viral or bacterial DNA, as well as DNA released from mitochondria or dead cells[35]. Nonetheless, these DNAs are not suitable for *in vivo* STING activation, for their poor penetration ability and low efficacy.

The activation of STING largely depends on the role of cGAS, an enzyme that catalyzes the formation of cGAMP from GMP and AMP. It is reported that dsDNA activates cGAS in a size-dependent manner, and only those dsDNA with a length more than 20 bp can induce the phase separation of cGAS and sequential activation[36]. In the present study, we constructed five types of TDNs with distinct sizes and DNA sequences (T7, T13, T17, T26, and T37), and demonstrated that T17 displayed the highest efficiency in promoting STING activation and *Ifnb* production. These results indicated that TDNs activated STING in a size-dependent manner, but this effect of TDNs had nothing to do with their DNA sequence. Since the cell entrance efficacy of all the five TDNs was comparable, we speculated that the size of T17 may be the most suitable to the DNA binding site of STING.

Several divalent metal cations have been reported to participate in modulating immune response. For example, Ca^{2+} functions as an intracellular second messenger to enhance signal transduction. Mn^{2+} dramatically increases the sensitivity of cGAS to dsDNA and promoted STING activation[14]. Whereas Mg^{2+} promotes the recruitment and polarization of monocytes/macrophages, and slightly up-regulates cGAS-STING activation[23]. Our results demonstrated that at a concentration of 25 or 50 μmol/L, only Mn^{2+} displayed a synergy with TDN in promoting *Ifnb*, *Isg15* and *Inos* expression. A recent study by Chen et al.[37] presented a Mn-cGAMP nano vaccine (NVs) to direct cytosolic co-delivery of cGAMP and Mn^{2+} to potentiate the anti-tumor immune response. Our studies demonstrated that Mn^{2+} and TDNs not only synergistically strengthened the activation of STING/type I IFN pathway, but also promoted the M1 polarization and antigen presentation in primary macrophages. The data showed that T17-induced M1 polarization partially depended on STING, indicating that T17 might activate other pathways leading to M1 polarization. It is reported that activation of other DNA sensors such as TLR9, AIM2, LRRFIP1, DAI, sometimes also contribute to NF-κB activation, Type I IFN production, or M1 polarization, and this process is independent of STING[38–42]. Since STING is the central molecule of various DNA receptor pathways, we speculate that the T17-induced M1 polarization is mainly dependent on STING.

To be noted, studies have demonstrated that an excess or accumulation of manganese is harmful to the central nervous system[15]. Our results also confirmed the cytotoxicity of Mn^{2+} at a concentration of 100 μmol/L *in vitro*. A recent study by Lv group[14] demonstrated that manganese promotes anti-tumor response by increasing the cGAS/STING activation. In their study, mice received continuous treatment of Mn^{2+} (5 mg/kg) before tumor growth (which mimics a tumor vaccine model), and the results show that Mn^{2+} prevents tumor growth and promotes anti-tumor response[14]. However, in the Hepa1-6 tumor model of our study, mice were treated with Mn^{2+} (30 mg/kg) or MnO_2 (0.867 mg/kg) for three times after the tumors had grown to a certain size more than 50 mm^3 (which mimics a tumor treatment model). Our results demonstrated that treatment with Mn^{2+} alone had no obvious effect in restricting tumor growth, which may correlate to the side effects of Mn^{2+} at a high concentration. Therefore, we constructed manganese dioxide (MnO_2) nanosheets, which release the Mn^{2+} in a GSH-enriched environment such as TME. Recently, Yang et al.[43] developed an *in situ* STING activating vaccination (ISSAV), by using cancer cell membrane (CM) to encapsulate manganese dioxide nanoparticles and immobilize photothermal agent, and showed the design facilitated TAAs and DAMPs released from dying cells under laser irradiation, increased the pH value of TME and created a favorable environment for T cell infiltration. In the present study, T17 was incubated with MnO_2 nanosheet to assemble the T17-MnO_2 nanostructure, and both *in vivo* and *in vitro* studies suggested that T17-MnO_2 displayed a much higher efficiency in triggering STING/type I IFN signal activation, M1 polarization as well as antigen presentation. More importantly, in mice-bearing Hepa1-6 xenograft, intratumor injection of T17-MnO_2 achieved more efficient anti-tumor effects than T17 plus Mn^{2+}, although the concentration of manganese applied in the latter group was twenty-five times more than that in T17-MnO_2 group. Two possible mechanisms may explain the better synergy of T17-MnO_2 in anti-tumor immunity. Firstly, Zhao et al.[44] demonstrated that Mn^{2+} bind to the active site of cGAS to induce STING activation. After the assembly of T17-MnO_2, T17 attached to the surface of MnO_2 nanosheet (a controlled release system of Mn^{2+})[45], thereby increasing the local concentration of T17 and Mn^{2+} to promote a sustained and stronger activation of STING pathways. Secondly, Mn^{2+} displays a neurotoxic effect at a high concentration[15], while MnO_2 can react with glutathione (GSH) that is high in the tumor microenvironment, to produce Mn^{2+} in a sustained release manner[45]. This advantage of MnO_2 can limit the side effects of *in vivo* application of manganese at a high concentration.

Consistently, among all the indicated treatment with TDN and/or manganese, T17-MnO_2 displayed the most potent ability to reprogram TAM polarization from the tumor-promoting M2 type to the tumor-killing M1 type, thereby boosting both innate and adaptive anti-tumor immune responses.

5. Conclusions

Summarily, our study demonstrated a synergy of TDNs and manganese in triggering STING activation, *Ifnb*/*Isg*s production, M1 polarization and antigen presentation. This TDN-mediated macrophage activation was influenced by the TDN size, rather than DNA sequence. Moreover, compared to TDN plus Mn^{2+}, MnO_2 nanosheet with TDN displayed a much stronger synergy to promoting macrophage activation and host anti-tumor response. Therefore, our findings offered a novel anti-tumor immunotherapy strategy based on STING-mediated TAM reprogramming.

Acknowledgments

This work was supported by grants: National Natural Science Foundation of China (82072087, 31670880 and 31970893, China); Guangdong Natural Science Fund for Distinguished Young Scholars (2017A030306016 and 2016A030306004, China); the Fundamental Research Funds for the Central Universities (19ykzd39, China); Open project of Guangdong Key Laboratory of Chiral Molecule and Drug Discovery (Sun Yat-sen University, China).

Author contributions

Minhao Wu, Yuanqing Zhang and Jiaping Li designed the research. Siping Liang and Jiaying Li carried out the experiments

and performed data analysis. Zhengyu Zou, Miao Mao, Siqi Ming, Fan Lin, Ziyan Zhang, Can Cao and Jinyu Zhou participated part of the experiments. Siping Liang and Minhao Wu wrote the manuscript. Siping Liang, Minhao Wu, Yuanqing Zhang and Jiaping Li revised the manuscript. All of the authors have read and approved the final manuscript.

Conflicts of interest

The authors have no conflicts of interest to declare.

Appendix A. Supporting information

Supporting data to this article can be found online at https://doi.org/10.1016/j.apsb.2021.12.010.

References

1. Corrales L, Matson V, Flood B, Spranger S, Gajewski TF. Innate immune signaling and regulation in cancer immunotherapy. *Cell Res* 2017;**27**:96−108.
2. Ruffell B, Coussens LM. Macrophages and therapeutic resistance in cancer. *Cancer Cell* 2015;**27**:462−72.
3. Guillerey C, Huntington ND, Smyth MJ. Targeting natural killer cells in cancer immunotherapy. *Nat Immunol* 2016;**17**:1025−36.
4. Bellmunt J, Powles T, Vogelzang NJ. A review on the evolution of PD-1/PD-L1 immunotherapy for bladder cancer: the future is now. *Cancer Treat Rev* 2017;**54**:58−67.
5. Gong J, Chehrazi-Raffle A, Reddi S, Salgia R. Development of PD-1 and PD-L1 inhibitors as a form of cancer immunotherapy: a comprehensive review of registration trials and future considerations. *J Immunother Cancer* 2018;**6**:8.
6. Doroshow DB, Bhalla S, Beasley MB, Sholl LM, Kerr KM, Gnjatic S, et al. PD-L1 as a biomarker of response to immune-checkpoint inhibitors. *Nat Rev Clin Oncol* 2021;**18**:345−62.
7. Kottke T, Evgin L, Shim KG, Rommelfanger D, Boisgerault N, Zaidi S, et al. Subversion of NK-cell and TNFα immune surveillance drives tumor recurrence. *Cancer Immunol Res* 2017;**5**:1029−45.
8. Rodriguez-Garcia A, Lynn RC, Poussin M, Eiva MA, Shaw LC, O'Connor RS, et al. CAR-T cell-mediated depletion of immunosuppressive tumor-associated macrophages promotes endogenous antitumor immunity and augments adoptive immunotherapy. *Nat Commun* 2021;**12**:1−17.
9. Borden EC. Interferons alpha and beta in cancer: therapeutic opportunities from new insights. *Nat Rev Drug Discov* 2019;**18**:219−34.
10. Woo SR, Fuertes MB, Corrales L, Spranger S, Furdyna MJ, Leung MY, et al. STING-dependent cytosolic DNA sensing mediates innate immune recognition of immunogenic tumors. *Immunity* 2014;**41**:830−42.
11. Ma Z, Damania B. The cGAS-STING defense pathway and its counteraction by viruses. *Cell Host Microbe* 2016;**19**:150−8.
12. Kwon J, Bakhoum SF. The cytosolic DNA-sensing cGAS-STING pathway in cancer. *Cancer Discov* 2020;**10**:26−39.
13. Yum SY, Li MH, Chen ZJ. Old dogs, new trick: classic cancer therapies activate cGAS. *Cell Res* 2020;**30**:639−48.
14. Lv MZ, Chen MX, Zhang R, Zhang W, Wang CG, Zhang Y, et al. Manganese is critical for antitumor immune responses *via* cGAS-STING and improves the efficacy of clinical immunotherapy. *Cell Res* 2020;**30**:966−79.
15. Martinez-Finley EJ, Gavin CE, Aschner M, Gunter TE. Manganese neurotoxicity and the role of reactive oxygen species. *Free Radic Biol Med* 2013;**62**:65−75.
16. Wang Y, Luo JW, Alu A, Han XJ, Wei YQ, Wei XW. cGAS-STING pathway in cancer biotherapy. *Mol Cancer* 2020;**19**:136.
17. Seeman NC. Nucleic acid junctions and lattices. *J Theor Biol* 1982;**99**:237−47.
18. Zhang T, Tian TR, Zhou RH, Li SH, Ma WJ, Zhang YX, et al. Design, fabrication and applications of tetrahedral DNA nanostructure-based multifunctional complexes in drug delivery and biomedical treatment. *Nat Protoc* 2020;**15**:2728−57.
19. Zhu JY, Zhang M, Gao Y, Qin X, Zhang TX, Cui WT, et al. Tetrahedral framework nucleic acids promote scarless healing of cutaneous wounds *via* the AKT-signaling pathway. *Signal Transduct Target Ther* 2020;**5**:1−11.
20. Liu NX, Zhang XL, Li N, Zhou M, Zhang TX, Li SH, et al. Tetrahedral framework nucleic acids promote corneal epithelial wound healing *in vitro* and *in vivo*. *Small* 2019;**15**:e1901907.
21. Shao XR, Lin SY, Peng Q, Shi SR, Wei XQ, Zhang T, et al. Tetrahedral DNA nanostructure: a potential promoter for cartilage tissue regeneration *via* regulating chondrocyte phenotype and proliferation. *Small* 2017;**13**:1602770.
22. Zhang Q, Lin SY, Shi SR, Zhang T, Ma QQ, Tian TR, et al. Anti-inflammatory and antioxidative effects of tetrahedral DNA nanostructures *via* the modulation of macrophage responses. *ACS Appl Mater Interfaces* 2018;**10**:3421−30.
23. Wang CG, Guan YK, Lv MZ, Zhang R, Guo ZY, Wei XM, et al. Manganese increases the sensitivity of the cGAS-STING pathway for double-stranded DNA and is required for the host defense against DNA viruses. *Immunity* 2018;**48**:675−87.
24. Marchi S, Giorgi C, Galluzzi L, Pinton P. Ca^{2+} fluxes and cancer. *Mol Cell* 2020;**78**:1055−69.
25. Liu Y, Yan W, Tohme S, Chen M, Fu Y, Tian D, et al. Hypoxia induced HMGB1 and mitochondrial DNA interactions mediate tumor growth in hepatocellular carcinoma through Toll-like receptor 9. *J Hepatol* 2015;**63**:114−21.
26. Zhang XW, Zhang P, An L, Sun NY, Peng LY, Tang WW, et al. Miltirone induces cell death in hepatocellular carcinoma cell through GSDME-dependent pyroptosis. *Acta Pharm Sin B* 2020;**10**:1397−413.
27. Galon J, Bruni D. Approaches to treat immune hot, altered and cold tumours with combination immunotherapies. *Nat Rev Drug Discov* 2019;**18**:197−218.
28. Bassez A, Vos H, Van Dyck L, Floris G, Arijs I, Desmedt C, et al. A single-cell map of intratumoral changes during anti-PD1 treatment of patients with breast cancer. *Nat Med* 2021;**27**:820−32.
29. Fuertes MB, Kacha AK, Kline J, Woo SR, Kranz DM, Murphy KM, et al. Host type I IFN signals are required for antitumor $CD8^+$ T cell responses through $CD8\alpha^+$ dendritic cells. *J Exp Med* 2011;**208**:2005−16.
30. Marcus A, Mao AJ, Lensink-Vasan M, Wang L, Vance RE, Raulet DH. Tumor-derived cGAMP triggers a STING-mediated interferon response in non-tumor cells to activate the NK cell response. *Immunity* 2018;**49**:754−63.
31. Jiang ML, Chen PX, Wang L, Li W, Chen B, Liu Y, et al. cGAS-STING, an important pathway in cancer immunotherapy. *J Hematol Oncol* 2020;**13**:81.
32. Zhou C, Chen X, Planells-Cases R, Chu JC, Wang L, Cao LM, et al. Transfer of cGAMP into bystander cells *via* LRRC8 volume-regulated anion channels augments STING-mediated interferon responses and anti-viral immunity. *Immunity* 2020;**52**:767−81.
33. Chen L, Zhang J, Lin Z, Zhang ZY, Mao M, Wu JC, et al. Pharmaceutical applications of framework nucleic acids. *Acta Pharm Sin B* 2022;**12**:76−91.
34. Ruoslahti E. Tumor penetrating peptides for improved drug delivery. *Adv Drug Deliv Rev* 2017;**110−111**:3−12.
35. Hopfner KP, Hornung V. Molecular mechanisms and cellular functions of cGAS-STING signalling. *Nat Rev Mol Cell Biol* 2020;**21**:501−21.

36. Du M, Chen ZJ. DNA-induced liquid phase condensation of cGAS activates innate immune signaling. *Science* 2018;**361**:704−9.
37. Chen CY, Tong YH, Zheng YS, Shi YJ, Chen ZW, Li J, et al. Cytosolic delivery of thiolated Mn-cGAMP nanovaccine to enhance the antitumor immune responses. *Small* 2021;**17**: e2006970.
38. Kumagai Y, Takeuchi O, Akira S. TLR9 as a key receptor for the recognition of DNA. *Adv Drug Deliv Rev* 2008;**60**:795−804.
39. Wang J, Li RT, Peng ZY, Hu B, Rao X, Li JG. HMGB1 participates in LPS-induced acute lung injury by activating the AIM2 inflammasome in macrophages and inducing polarization of M1 macrophages *via* TLR2, TLR4, and RAGE/NFkappaB signaling pathways. *Int J Mol Med* 2020;**45**:61−80.
40. Yang P, An H, Liu X, Wen M, Zheng Y, Rui Y, et al. The cytosolic nucleic acid sensor LRRFIP1 mediates the production of type I interferon *via* a beta-catenin-dependent pathway. *Nat Immunol* 2010; **11**:487−94.
41. Takaoka A, Wang ZC, Choi MK, Yanai H, Negishi H, Ban T, et al. DAI (DLM-1/ZBP1) is a cytosolic DNA sensor and an activator of innate immune response. *Nature* 2007;**448**:501−5.
42. Wang N, Liang HW, Zen K. Molecular mechanisms that influence the macrophage M1–M2 polarization balance. *Front Immunol* 2014;**5**:614.
43. Yang X, Yang Y, Bian JY, Wei JJ, Wang Z, Zhou ZW, et al. Converting primary tumor towards an *in situ* STING-activating vaccine *via* a biomimetic nanoplatform against recurrent and metastatic tumors. *Nano Today* 2021;**38**:101109.
44. Zhao Z, Ma ZX, Wang B, Guan YK, Su XD, Jiang ZF. Mn^{2+} directly activates cGAS and structural analysis suggests Mn^{2+} induces a noncanonical catalytic synthesis of 2′3′-cGAMP. *Cell Rep* 2020;**32**:108053.
45. Wang YW, Li YM, Zhang ZJ, Wang L, Wang D, Tang BZ. Triple-jump photodynamic theranostics: MnO_2 combined upconversion nanoplatforms involving a Type-I photosensitizer with aggregation-induced emission characteristics for potent cancer treatment. *Adv Mater* 2021:**33**e2103748.